ACS APPLIED MATERIALS & INTERFACES

www.acsami.org

Forum Article

Additive Manufacture of Dynamic Thiol−ene Networks Incorporating Anhydride-Derived Reversible Thioester Links

Maciej Podgórski, Sijia Huang, and Christopher N. Bowman*

Cite This: *ACS Appl. Mater. Interfaces* 2021, 13, 12789−12796

Read Online

ACCESS | Metrics & More | Article Recommendations | Supporting Information

ABSTRACT: A photoprintable dynamic thiol−ene resin was developed based on commercially available anhydride, thiol, and ene monomers. The dynamic chemistry chosen for this study relied on the thermal reversibility of the in situ generated thioester-anhydride links. The resin's rheological and curing properties were optimized to enable 3D printing using the masked stereolithography (MSLA) technique. To achieve a desirable depth of cure of 200 μm, a combination of radical photoinitiator (BAPO) and inhibitor (pyrogallol) were used at a weight ratio of 0.5 to 0.05, resulting in more than 90% thiol−ene conversion within 12 s curing time. In a series of stress relaxation and creep experiments, the dynamic reversible exchange was characterized and yielded rapid exchange rates ranging from minutes to seconds at temperatures of 80−140 °C. Little to no exchange was observed at temperatures below 60 °C. Various 3D geometries were 3D printed, and the printed objects were shown to be reconfigurable above 80 °C and depolymerizable at or above 120 °C. By deactivation of the exchange catalyst (DMAP), the stimuli responsiveness was demonstrated to be erasable, allowing for a significant shift in the actuation threshold. These highly enabling features of the dynamic chemistry open up new possibilities in the field of shape memory and 4D printable functional materials.

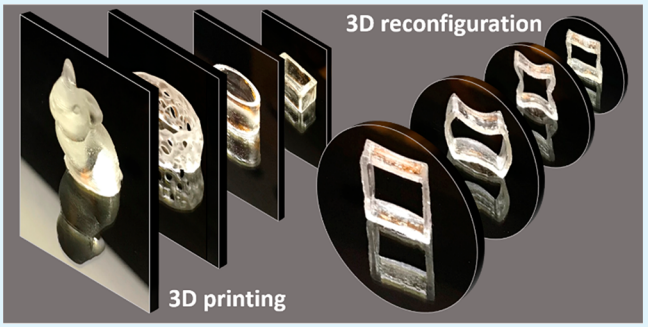

KEYWORDS: *3D printing, 4D printing, photopolymerization, covalent adaptable networks, stress relaxation*

INTRODUCTION

Fabricating covalent adaptable networks (CANs) with the use of additive manufacturing techniques effectively combines the beneficial features of the two rapidly growing disciplines of materials science and engineering. Such close association of concepts gives rise to a new quality where the creation of complex three-dimensional geometries is achieved with an inherent ability for subsequent changes in shape, functionality, and properties, typically upon application of an external stimulus.[1] In a broader context, achieving new functionality postprinting is referred to as 4D printing as there exists a "fourth dimension", i.e., the time postponed material activation or actuation step.[2,3]

Although the concept of 4D printing has expanded in recent years and involves a wide range of active polymers, including shape memory polymers, hydrogels, and liquid crystal elastomers,[4−10] the existence of dynamic covalent bonds has implications well beyond these fields and applications. It is in accordance with sustainability demands that are compromised in most nondynamic thermosets. Direct reprocessing and end-of-life depolymerization and recycling, not to mention extended life cycles achieved by self-repair or self-healing, are the attributes of immeasurable impact on the environment.[11] To this end, the reprocessing and self-healing of printed structures has been realized with the use of transesterification,[12,13] imine exchange,[14] or Diels−Alder reactions,[15] to name a few. Although many of the transformations of the printed structures have been realized with noncovalent interactions, e.g., by introducing ureido-pyrimidinone motifs (UPyMA) capable of hydrogen bonding[4] or by physical phenomena such as stress-driven reshaping resulting from gradient material heterogeneities,[16] or selective removal of monomer from the printed structures,[5] the incorporation of dynamic covalent chemistries (DCCs) seems particularly enabling in tuning of the properties and actuation methods. In biomedical fields, the 3D printing of dynamic hydrogels provides unprecedented opportunities in designing of responsive scaffolds for tissue engineering applications.[17] For example, the dynamic hydrazone chemistry[18] and coumarin [2 + 2] reversible photoadditions[19] have been shown to fit the purpose well. Other CANs have been printed incorporating dynamic exchange of imine bonds,[20] urea bonds,[21] trithiocarbonates,[22] or allyl sulfides.[23] Intricate postprinting trans-

Special Issue: Novel Stimuli-Responsive Materials for 3D Printing

Received: October 22, 2020
Accepted: December 9, 2020
Published: December 23, 2020

https://dx.doi.org/10.1021/acsami.0c18979
ACS Appl. Mater. Interfaces 2021, 13, 12789−12796

formations have been demonstrated, often with the incorporation of liquid crystal domains to enable even more dramatic shape-morphing characteristics.

Three-dimensional printing technologies continually evolve to bring innovations to the printing process itself and to the final characteristics of the material and device.[24−26] Particularly enabling are photo-3D printing methods.[27] Digital light processing (DLP) and stereolithography (SLA) are the two most common 3D photopolymerization techniques, and either one offers advantages for specific printing needs as well as commercially available, low-cost printers. Other innovative methods for the fabrication of complex 3D systems with controllable optical, chemical, and mechanical properties are based on continuous liquid interface production (CLIP), which achieves high printing speeds as well as eliminates the anisotropy in properties typically seen in layer-by-layer fabricating methods.[28] Two-photon polymerization approaches further allow for high precision in printing of micro- and nanosized objects.[29] Technical innovations of the photoprinting processes often limit the applicability of photocurable resins to only a particular resin type or in other cases affect the achievable resolution of the printed geometries. To date, the majority of photoprinted materials are based on (meth)acrylate or epoxy photopolymerizations.[30−36]

To further expand the scope of photoprintable and stimuli-responsive resins, we introduced a thioester-anhydride dynamic reversible chemistry into a thiol−ene photopolymerizable system. In this report, the rheological and photocuring properties of elastomeric thiol−ene materials were optimized for masked SLA 3D photopolymerization with visible light. The temperature responsiveness of the dynamic elastomers with introduced compositional variations is quantified in thermally induced stress relaxation and creep experiments. Further, various decorative and functional 3D geometries were printed, and the existence of reversible exchange was explored for material depolymerization and recycling as well as thermal reshaping and shape fixation by the deactivation of the exchange catalysts in the printed objects. Through the catalyst deactivation, the shift in the DCC activation threshold was also demonstrated.

EXPERIMENTAL SECTION

Materials and Methods. All chemicals were purchased from common suppliers (Sigma-Aldrich, Fisher Scientific, Bruno Bock, Alpha Aesar) and used as received. Radical photoinitiators and inhibitors: 2,2-dimethoxy-2-phenylacetophenone (DMPA), phenylbis(2,4,6-trimethylbenzoyl)phosphine oxide (BAPO), and pyrogallol (PYR). Reactants and monomers: (99%) allyl succinic anhydride (ASA) (98%), trimethylolpropane tris(3-mercaptopropionate) (TMPTMP), 1,6-hexanedithiol (HDT), 1,3,5-triallyl-1,3,5-triazyne-2,4,6-trione (TTT), diallyl carbonate (DAC), allyl ether (AE), diallyl terephthalate (DATP), hydrochloric acid (37%), and sulfuric acid (98%). Organic catalysts and solvents: methylene chloride (DCM), acetone, and 4-dimethylaminopyridine (DMAP).

Sample Casting and Depolymerization. The reactants (allyl anhydride, thiol, and/or diallyl) were mixed at room temperature and the catalyst/photoinitiator/inhibitor mixture was added in a DCM solution. After 10−30 min of initial reaction, the solvent was removed in vacuo, and the mixture casted between glass slides separated by spacers (typically 250 μm thick). After 1 h of the thiol-anhydride reaction, the mixtures were exposed to UV irradiation at 0.5 mW/cm^2 (365 nm) or visible light irradiation (0.5 mW/cm^2, 405 nm) to form cross-linked dynamic networks. The first-step thiol-anhydride reaction was carried out for an extended time prior to photocuring to allow for maximum attainable thioester formation. The initially rapid ring opening reaction decelerates significantly with increasing viscosity and reaches around 85% conversion in 1 h reaction time (Figure S1). The extent of anhydride ring opening reaction was monitored by ATR-IR spectroscopy. Depolymerization was achieved by gradually reacting the dynamic polymer with a fresh mixture of excess monomers (typically equivalent amount/weight in respect to the amount of recycled material) at 120 °C for up to 30 min. After complete solubilization, additional amounts of DMAP, and photoinitiator were added in DCM. The total DMAP concentration in the recycled samples was 5 mol % with respect to the thioester content.

DCC Deactivation. Photopolymerized samples and/or the printed objects were swollen in acetone for 10 min. After swelling, which resulted in around 10 wt % sample mass increase, the samples were kept in a hydrogen chloride atmosphere for 30 min. The HCl_g was generated by adding dropwise hydrochloric acid into sulfuric acid. After 30 min of contact with HCl_g, the samples were directly used for testing. The 3D prints were dried for another 30 min at 60 °C.

Shape Reconfiguration. The 3D prints were deformed to the desired new shapes, and while at constrained configurations exposed to elevated temperatures (85, 120, and 140 °C) for a given amount of time (30 min.). After the constraint was removed, the final shapes in the new configurations were obtained.

Fourier Transform Infrared Spectroscopy. Sample conversions were analyzed using an FT-IR spectrometer (Nicolet 8700) equipped with an ATR accessory. Monomer mixtures were deposited on the ATR crystal window, whereas the 250 μm thick films were pressed against it before scanning. Uncured resin mixtures and photocured samples of fixed geometries (5 mm/15 mm/0.25 mm) were surface-analyzed in ATR-IR where the highest peak absorbance was set to 0.6. Real time conversion analysis was performed in a horizontal transmission apparatus where the liquid samples were continually scanned during UV and visible light exposures at 0.5 mW/cm^2 (365 and 405 nm) for 5 min. The final double bond conversions were calculated from the absorbance peak area of the vinyl functional group, around 6120 cm^{-1} in the near-infrared spectrum.

Dynamic Mechanical Analysis (DMA), Stress Relaxation, and Creep. The glass transition temperature (T_g), storage modulus (E'), loss modulus (E''), and tangent δ were determined on a Q800 DMA (TA Instruments) using a ramp rate of 3 °C/min and a frequency of 1 Hz, with a fixed oscillatory strain of 0.01% and a preload force of 0.002 N. Stress relaxation experiments were performed in tensile elongation mode using a Q800 DMA instrument. The built-in stress relaxation DMA setting was used, with a 5−8% maximal strain and an initial strain rate of 1%/s at a fixed temperature. Rectangular samples of the dimensions 10/4/0.20 were used. Creep tests were performed in tensile elongation mode. A constant stress was applied at fixed temperatures, and the strain was monitored for 10−30 min. Depending on the temperature, a stress of 100 to 600 kPa was applied which resulted in 2−15% initial sample elongation. The resin viscosities were measured using ARES G2 Rheometer (TA Instruments) with a 200 s^{-1} shear rate and operating gap of 0.2 mm.

3D Printing. A Prusa SL1 3D printer was used to create the layer-by-layer projected geometries. It utilizes the masked SLA technique with an LED array as its light source and an LCD photomask to shape the light image from the LED array. The image is digitally displayed across the platform and is similar to single image projections from a DLP-SLA technique. The nominal light intensity was 0.4 mW/cm^2 at the surface of the window, whereas the wavelength was 405 nm. The photoprinted objects were washed with acetone and subsequently flood-cured at 10 mW/cm^2 with a broad range UV light for 5 min.

RESULTS AND DISCUSSION

Recently, thioester-anhydride based CANs were fabricated with the use of various commercial and synthetic anhydrides and multifunctional mercaptopropionates.[37,38] This new dynamic chemistry has been shown to have highly tunable reversible exchange characteristics. The thioester-anhydride networks were synthesized by a direct ring opening reaction of the anhydride and thiol reactants. The process was facilitated

https://dx.doi.org/10.1021/acsami.0c18979
ACS Appl. Mater. Interfaces 2021, 13, 12789−12796

Scheme 1. Methodology of Thiol−ene CANs Preparation[a]

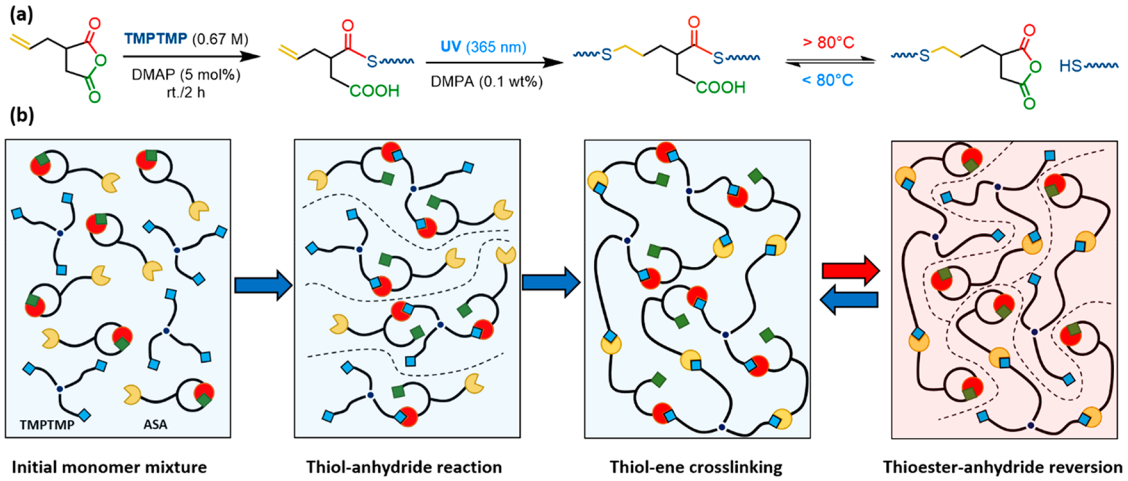

[a](a) Chemical equations showing products of the thiol-anhydride reaction, thiol−ene polymerization and crosslinking and thioester-anhydride reversion above 80 °C; (b) a schematic depicting CAN formation and depolymerization. The functional groups are color-coded (thiol, blue; double bond, yellow; carboxylic group, green; thioester, red and blue; anhydride, red and green; sulfide, yellow and blue).

by inclusion of catalysts (bases and nucleophiles) and was found to be reversible at elevated temperatures, typically above 80 °C. Among various types of thioester-anhydride materials examples of thiol−ene photopolymers were also shown. Herein, the thioester-anhydride photopolymer CANs were developed for additive manufacture using the MSLA photo-printing technique. Allyl succinic anhydride (ASA) was initially reacted with trimethylolpropane tris(3-mercaptopropionate) (TMPTMP) in a mixture with a 2:1:1 stoichiometry of thiol to ene to anhydride functional groups (Scheme 1).

The initial resin mixture was characterized for its reaction kinetics (Figure 1a), and the resultant CAN was analyzed in DMA (Figures S2 and S3, Table 1). Inherently necessary in 3D photopolymerizations, the thiol−ene resin requires relatively low viscosity (<5 mPa s)[39] and rapid reaction kinetics, even at low light intensities (0.5 mW/cm^2). However, the anhydride ring opening increases the mixture viscosity due to the formation of oligomeric species as well as the release of free carboxylic groups (Scheme 1). To facilitate 3D printing, an attempt was made to modify the viscosity by inclusion of less viscous diallyl monomers. Accordingly, diallyl carbonate, allyl ether, and diallyl terephthalate were preselected and used with ASA and TMPTMP at a molar ratio of 2:2:1 of TMPTMP, ASA, and diallyl monomer, respectively. As predicted by the Flory−Stockmayer gelation theory, the gel point conversion of TMPTMP and diallyl at a molar ratio of 2 to 1 would be 1.22. Thus, no gelation would be expected. As such, in the presence of ASA, complete depolymerization, and in consequence, 100% stress relaxation, will be enabled. The inclusion of low viscosity alkenes reduced the viscosity by close to 1 order of magnitude (Table 1).

Although all three monomer modifications meet the initial viscosity criteria, the one with diallyl carbonate exhibited the lowest viscosity, and consequently, this resin was chosen for further optimization and 3D printing. In the literature, there are known examples of thiol−ene and thiol−yne photopolymerizations adapted for additive manufacture techniques.[40−43] Thiol−ene resins are characterized by rapid kinetics, which makes them excellent precursor components for photopolymer materials. The downside is that such resins tend to react spontaneously and therefore show poor storage

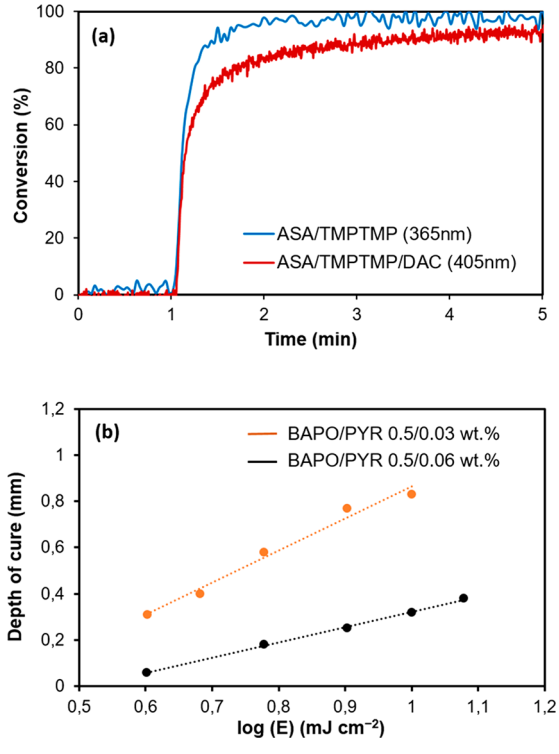

Figure 1. Kinetic characterization of thioester-anhydride resins. (a) Allyl functional group conversion vs time for ASA/PETMP initial formulation and ASA/TMPTMP/DAC optimized formulation (BAPO/PYR 0.5/0.05 wt %). The light intensities were 0.5 mW/cm^2 in both cases. (b) Curing depth as a function of dose (E) for ASA/TMPTMP/DAC with two concentrations of PYR and a constant concentration of initiator (0.5 wt %).

stability.[44] In photo-3D printing methodologies, to achieve a desired curing depth, researchers typically use light absorbers or radical inhibitors.[45] While enabling a controllable depth of cure, the inhibitors also improve the stability. It was previously demonstrated that the shelf life of thiol−ene systems is effectively extended in mixtures with secondary mercaptopropionates,[41] and by adding radical inhibitors such as pyrogallol

https://dx.doi.org/10.1021/acsami.0c18979
ACS Appl. Mater. Interfaces 2021, 13, 12789−12796

Table 1. Basic Properties of Dynamic Thiol−ene Resins and CANs[a]

resin	viscosity (mPa s)	T_g (°C)	relaxation time at e^{-1} (100 °C)
ASA/TMPTMP	11.8 (0.5)	21 (2)	26 s (−)
ASA/TMPTMP/AE	1.2 (0.1)	9 (1)	30 s (−)
ASA/TMPTMP/DATP	1.6 (0.1)	16 (1)	32 s (−)
ASA/TMPTMP/DAC	0.6 (0.1)	12 (2)	55 s−1 min 10 s

[a]SD values are in parentheses.

(PYR), often used with phosphoric acid coadditives.[46] Another important consideration is the extent of cure, which can be compromised in stabilized mixtures, even to the point of entirely disabled gelation. Consequently, a kinetic and depth of cure vs photodosage (E) study was conducted to optimize the curing behavior required in a specific MSLA printer (PRUSA SL1, visible light 0.4 mW/cm^2). BAPO (0.5 wt %) and pyrogallol were used as the visible light initiator and the inhibitor, respectively. In Figure 1b, the depth of cure as a function of dose is plotted for the two concentrations of the inhibitor (0.03 and 0.06 wt %). It is evident that different curing depths are reached with the same doses of light depending on the inhibitor loading. For example, to achieve a desired depth of cure of 200 μm, a dose of 6 mJ cm^{-2} is required at 0.06 wt % PYR loading which corresponds to 15 s irradiance time. To reduce further the exposure time from 15 to about 11−12 s for the targeted depth of cure, so as to avoid an overexposure, the pyrogallol amount was reduced from 0.06 to 0.05 wt %. This initiator/inhibitor ratio allowed for acceptable conversion (90%), which is well above the gelation point of the cross-linked system, at low light intensities as evidenced by the relevant kinetic profile in Figure 1a.

Having adjusted the resin curing parameters for the MSLA printer of choice, various decorative objects and functional shapes were conveniently photoprinted as displayed in Figure 2. Relatively small objects were printed with the purpose to shorten the printing time and reduce the resin volumes required. For example, the time required to print the structure in Figure 2a was 46 min (250 layers), whereas it took 28 min to print the ring in Figure 2b (160 layers). No visible shape distortions resulting from the volumetric shrinkage were noticed in the printed objects, which was attributed to the relatively low concentrations of photopolymerizable groups (1 mol of allyl per 407.1 g of resin) and the step-growth polymerization mechanism.

It was previously reported that the dynamic behavior of the thioester-anhydride CANs depends on the catalyst type and loading and that selected catalysts differently affect the exchange mode.[38] It was argued that bases in systems with excessive thiol functionalities may additionally enable associative thiol-thioester exchange, whereas nucleophiles would bias dissociative ring closure and thiol regeneration in stoichiometric systems (Scheme 1a). Herein, DMAP was used as the reversible exchange catalyst because of its favorable characteristics, i.e., good solubility, nonvolatility, catalytic effectiveness, and stable response over time. Having a nucleophilic character and relatively low pK_a (~9.6), DMAP would be primarily dictating the reversible exchange mode.

The dynamic properties of the 3D printable material were assessed in thermomechanical and stress relaxation experiments. In Figure 3, the DMA data and stress relaxation curves are presented for the optimized formulation after curing.

There are three DMA profiles in Figure 3a that correspond to originally made, fresh CAN sample; a photopolymer sample that has been recycled and contains 50% of the recycled material; and a sample where the catalyst was deactivated by treatment with HCl gas (see Experimental Section for details). It is evident that the original and partially recycled samples are almost identical in their thermomechanical characteristics. Also, the samples with the deactivated catalyst exhibit similar DMA profiles, i.e., the glassy storage modulus, the rubbery storage modulus, and T_g are all close to other samples where the catalyst remains active. The DMAP, being mildly basic, is assumed to be deactivated through the acid−base association with HCl_g because of the significant differences in pK_a values. The presence of ionic or ion pair species in the network after deactivation seems to reinforce its structure to an extent as seen in the narrowing of the tan delta and a slight shift in the T_g. It was previously shown that DMAP can have a plasticizing effect on the polymethacrylate thioester-based networks.[47] However, when its nucleophilic attraction toward thioester carbonyls is broken down by deactivation, some reinforcing of the network would be expected. More importantly, the fabricated photopolymer was highly dynamic and capable of 100% stress relaxation in around 6 min at 100 °C (Figure 3b), which is consistent with previously reported data.[38] This relaxation time still be reduced to seconds at higher temperatures (Figure S4). As seen from Figure 3b, the recycled material exhibits an identical stress relaxation rate,

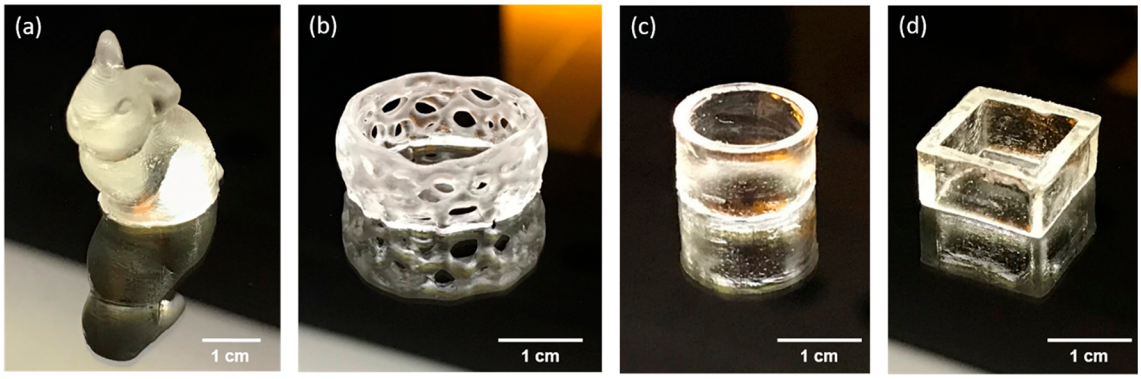

Figure 2. 3D prints fabricated using ASA/TMPTMP/DAC formulation: (a) bunny; (b) 3D decorative ring; (c) 3D plain ring; (d) 3D square ring. Initiator/inhibitor ratio 0.5/0.05 wt %. MSLA light intensity was 0.4 mW/cm^2.

https://dx.doi.org/10.1021/acsami.0c18979
ACS Appl. Mater. Interfaces 2021, 13, 12789−12796

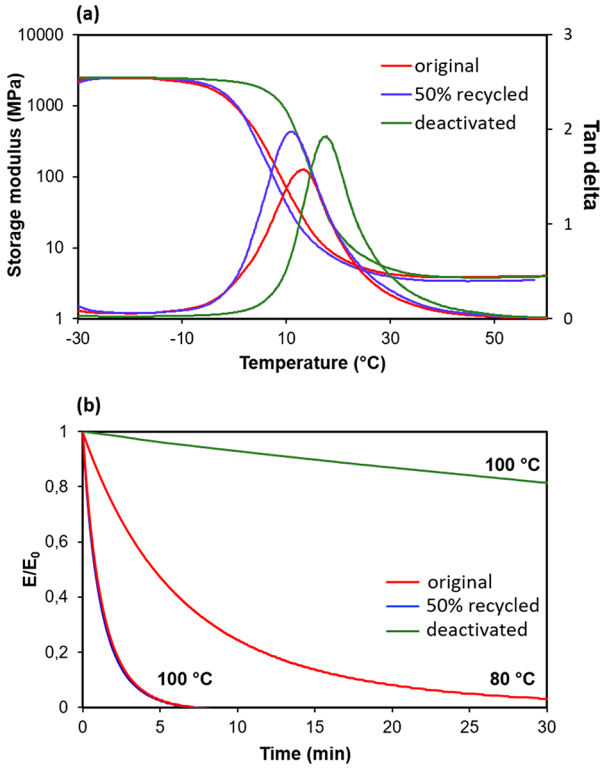

Figure 3. DMA data of the dynamic thioester-anhydride network. (a) Storage moduli and tangent delta plots for the thioester-anhydride neat sample, a sample composed of 50% recycled photopolymer and 50% fresh monomers, and a deactivated sample. (b) stress relaxation curves for the original photopolymer network and its recycled as well as deactivated analogs. Recycled samples perform comparatively with the original material. Postprocessed, i.e., HCl-deactivated samples exhibit similar thermomechanical characteristics but significantly reduced stress relaxation capability.

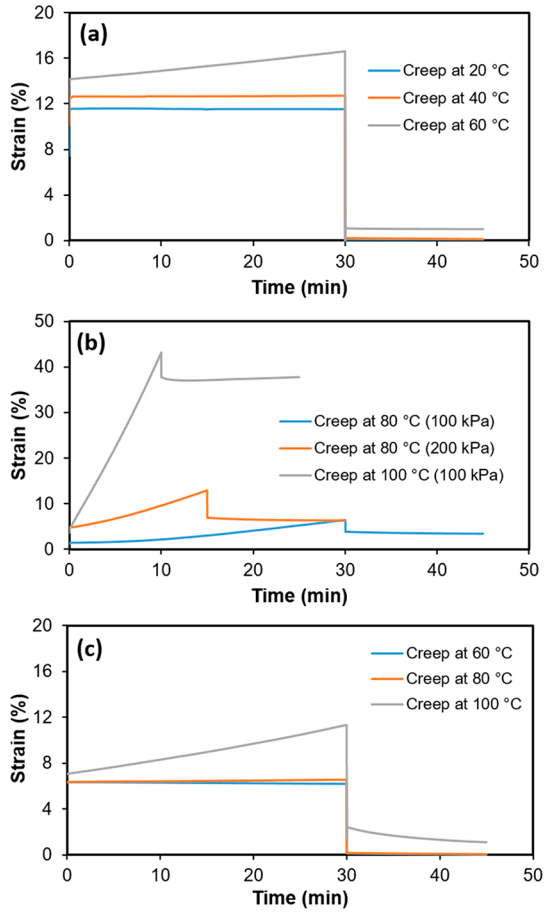

Figure 4. Creep experiments for the ASA/TMPTMP/DAC dynamic network. (a) Thirty minute creep results for samples deformed under 600 kPa stress at the temperatures from 20 to 60 °C; (b) 10−30 min creep results for samples deformed under 100−200 kPa stress at 80 and 100 °C; (c) 30 min creep data for deactivated specimens deformed under 300 kPa stress at the temperatures from 60 to 100 °C. The final strains vary for the samples analyzed at different creep temperatures and are dependent on the degree of activity of the dynamic chemistry. When the stress is released, the amount of strain adaptation is also correlated to the creep time. Deactivation of the catalysts inhibits creep that is otherwise very significant above 80 °C in samples with active catalyst.

pointing to a stable response over time and overall good repeatability. On the other hand, the catalyst deactivation resulted in drastic reduction of the material's dynamic response and stress relaxation capabilities. After deactivation the thioester-anhydride CAN dissipates only around 20% of the externally imposed stresses in 30 min at 100 °C. Such means of control over the dynamic responsiveness is a very useful feature as is demonstrated further in this study. Before the demonstration of the thermally induced responsiveness of the functional 3D prints, the creep data were collected and compared, especially between the dynamically active and inactive materials (Figure 4).

As shown in Figure 4a, there is little to no creep observed in the CAN system studied at temperatures below 60 °C. This is a temperature range where the network is constantly above its glass transition with no mobility restrictions on the functional groups or network chains and dynamic links. Yet, in the time scale of the experiments, at up to 40 °C, the material completely recovers its original shape (length). There is, however, close to 2% permanent deformation seen after 30 min at a constant stress at 60 °C. Above 80 °C the material becomes highly dynamic, and at 100 °C creep is so significant that the material rapidly adapts to nearly any stress induced deformation (Figure 4b). Finally, the process of exchange deactivation shifts the network rearrangement activation threshold up by around 40 °C. Such a conclusion is made by comparing the creep profiles at 60 and 100 °C in Figure 4a, c. In either case, similar strain loss is observed after the stress is released. Importantly, there is no visible activity of the DCC at 80 °C, where 100% of stress-induced strain is recovered.

Having determined the full potential for reversible exchange of the thioester-anhydride CANs, the 3D printed structures were then used for shape reconfiguration to illustrate the effectiveness and usefulness of such thermal responsiveness in these materials. Round and square-shaped objects were deformed at 85 °C for 30 min, resulting in new permanent shapes as illustrated in Figure 5. Once formed, the new shapes were geometrically reconfigured again as shown in a second reshaping cycle in Figure 5b. Importantly, when the DCC is deactivated, subsequent reconfiguration in shape is no longer possible at temperatures below 100 °C, and thus the fixed geometries remain stable and permanent. However, by increasing the temperature activation threshold to 140 °C, a complete shape restoration to its initial geometry was rendered within the 30 min of thermal annealing. To the best of our knowledge, the current approach is one rare example of

https://dx.doi.org/10.1021/acsami.0c18979
ACS Appl. Mater. Interfaces 2021, 13, 12789−12796

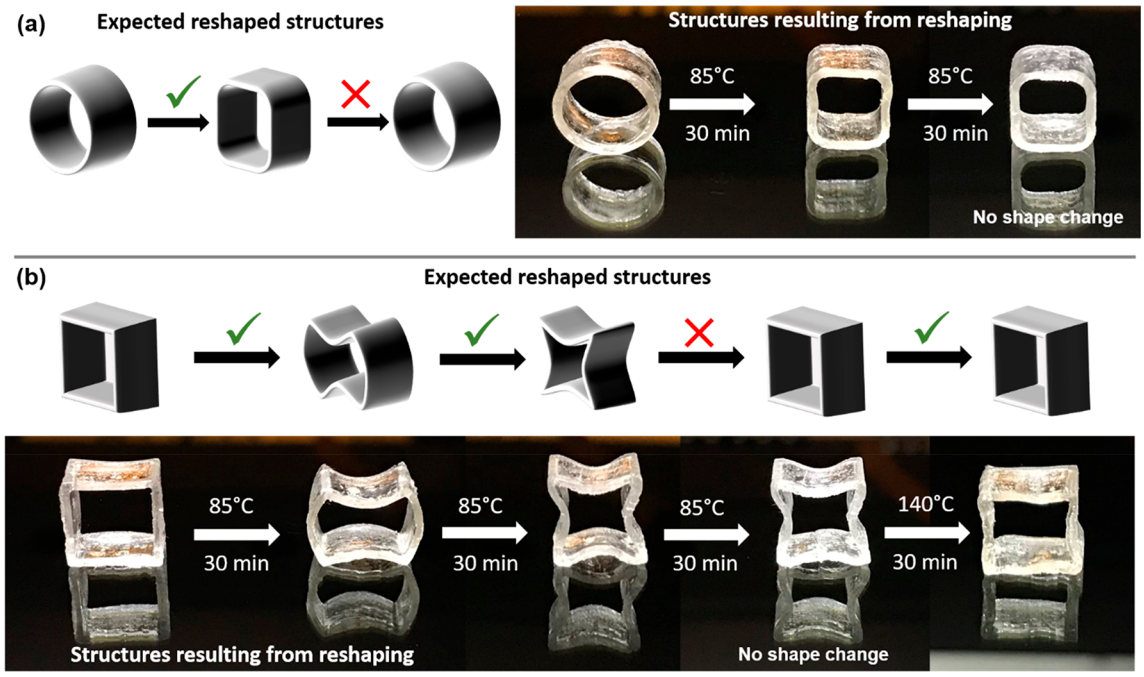

Figure 5. Shape change and restoration of the 3D printed geometries. (a) Round ring structure deformed and thermally reconfigured into a square-shaped ring following the DCC deactivation and shape fixation; (b) square-shaped 3D print reshaped into two consecutive permanent shapes, then fixed by DCC deactivation, and finally restored to its original shape by deformation and heating at 140 °C.

behavior where the DCC thermal activation is conveniently changed without any significant or detrimental effects on the network properties. The geometries of printed materials are facilely remodeled while having the ability to readily change the thermal activation threshold.

Partial shape reconfiguration was also demonstrated in semidynamic materials that were made by recycling the dynamic 3D printed components in a nondynamic thiol−ene resin (Figure S5). Prior to photocuring, the dynamic material was depolymerized in a dithiol followed by thiol−ene reaction with stoichiometric amount of the triene (TTT). Depending on the weight ratio of the dynamic CAN in a recycled photopolymer, various degrees of shape reconfigurations were thus achieved. This last demonstration serves as an example of convenient reprocessing of the 3D printed CAN through depolymerization and subsequent reuse in a form of mechanically distinct material with a varied degree of thermal responsiveness.

CONCLUSIONS

With the goal of adapting a new dynamic chemistry for additive manufacturing purposes, the thioester-anhydride thiol−ene photopolymer resin was developed from commercially available monomers and the resin's rheological and curing properties were optimized for MSLA printing under visible light. The stimuli responsiveness of the CAN material was tested in DMA stress relaxation and creep experiments providing rapid response at elevated temperatures (above 80 °C) and little to no response at temperatures below 60 °C. The activation threshold of the reversible exchange was shown to be controllable allowing for the shift in the actuation temperature by up to 40 °C. Such a degree of modulation or change in accessible activation mode resulted in 3D printed structures with variable thermal stabilities of their geometries depending on whether the DCC catalyst remained active or was rendered inactive. This useful feature of a DCC deactivation postprinting opens up new opportunities in 4D material development with two-way or multi shape memory effects, especially in hybrid or composite systems with programmable anisotropy of properties. Such chemistry may prove particularly enabling in materials incorporating liquid crystal domains. On the other hand, employing a dynamic resin such as the current one for additive manufacturing purposes may very well reduce or eliminate the anisotropy in properties resulting from layer-by-layer fabrication. Finally, any 3D geometries will be recyclable as previously demonstrated by direct reprocessing or as demonstrated here by depolymerization in excessive monomers and repolymerization leading to either retained or modified properties.

ASSOCIATED CONTENT

Supporting Information

The Supporting Information is available free of charge at https://pubs.acs.org/doi/10.1021/acsami.0c18979.

Additional graphics with FT-IR spectra, DMA data, stress relaxation data, and pictures of samples demonstrating partial reshaping capabilities (PDF)

AUTHOR INFORMATION

Corresponding Author

Christopher N. Bowman − *Department of Chemical and Biological Engineering, University of Colorado, Boulder, Colorado 80303, United States;* orcid.org/0000-0001-8458-7723; Email: Christopher.Bowman@colorado.edu

Authors

Maciej Podgórski − *Department of Chemical and Biological Engineering, University of Colorado, Boulder, Colorado 80303, United States; Department of Polymer Chemistry,*

https://dx.doi.org/10.1021/acsami.0c18979
ACS Appl. Mater. Interfaces 2021, 13, 12789−12796

Institute of Chemical Sciences, Faculty of Chemistry, Maria Curie-Sklodowska University, Lublin 20-031, Poland

Sijia Huang − *Department of Chemical and Biological Engineering, University of Colorado, Boulder, Colorado 80303, United States*

Complete contact information is available at: https://pubs.acs.org/10.1021/acsami.0c18979

Notes

The authors declare no competing financial interest.

■ ACKNOWLEDGMENTS

We acknowledge the support of the National Science Foundation (CHE 1808484).

■ REFERENCES

(1) Podgórski, M.; Fairbanks, B. D.; Kirkpatrick, B. E.; McBride, M.; Martinez, A.; Dobson, A.; Bongiardina, N. J.; Bowman, C. N. Toward Stimuli-Responsive Dynamic Thermosets through Continuous Development and Improvements in Covalent Adaptable Networks (CANs). *Adv. Mater.* **2020**, *32* (20), 1906876.

(2) Momeni, F.; M.Mehdi Hassani.N, S.; Liu, X.; Ni, J. A Review of 4D Printing. *Mater. Des.* **2017**, *122*, 42−79.

(3) González-Henríquez, C. M.; Sarabia-Vallejos, M. A.; Rodriguez-Hernandez, J. Polymers for Additive Manufacturing and 4D-printing: Materials, Methodologies, and Biomedical Applications. *Prog. Polym. Sci.* **2019**, *94*, 57−116.

(4) Invernizzi, M.; Turri, S.; Levi, M.; Suriano, R. 4D Printed Thermally Activated Self-healing and Shape Memory Polycaprolactone-based Polymers. *Eur. Polym. J.* **2018**, *101*, 169−176.

(5) Zhang, Y.; Huang, L.; Song, H.; Ni, C.; Wu, J.; Zhao, Q.; Xie, T. 4D Printing of a Digital Shape Memory Polymer with Tunable High Performance. *ACS Appl. Mater. Interfaces* **2019**, *11* (35), 32408−32413.

(6) Kuang, X.; Chen, K.; Dunn, C. K.; Wu, J.; Li, V. C. F.; Qi, H. J. 3D Printing of Highly Stretchable, Shape-Memory, and Self-Healing Elastomer toward Novel 4D Printing. *ACS Appl. Mater. Interfaces* **2018**, *10* (8), 7381−7388.

(7) Kuang, X.; Roach, D. J.; Wu, J.; Hamel, C. M.; Ding, Z.; Wang, T.; Dunn, M. L.; Qi, H. J. Advances in 4D Printing: Materials and Applications. *Adv. Funct. Mater.* **2019**, *29* (2), 1805290.

(8) Sossou, G.; Demoly, F.; Belkebir, H.; Qi, H. J.; Gomes, S.; Montavon, G. Design for 4D Printing: A Voxel-based Modeling and Simulation of Smart Materials. *Mater. Des.* **2019**, *175*, 107798.

(9) Kuang, X.; Qi, H. J. Modular 4D Printing Assisted by Dynamic Chemical Bonds. *Matter* **2020**, *2* (5), 1080−1082.

(10) Zhang, Q.; Kuang, X.; Weng, S.; Zhao, Z.; Chen, H.; Fang, D.; Qi, H. J. Rapid Volatilization Induced Mechanically Robust Shape-Morphing Structures toward 4D Printing. *ACS Appl. Mater. Interfaces* **2020**, *12* (15), 17979−17987.

(11) Fortman, D. J.; Brutman, J. P.; De Hoe, G. X.; Snyder, R. L.; Dichtel, W. R.; Hillmyer, M. A. Approaches to Sustainable and Continually Recyclable Cross-Linked Polymers. *ACS Sustainable Chem. Eng.* **2018**, *6* (9), 11145−11159.

(12) Shi, Q.; Yu, K.; Kuang, X.; Mu, X.; Dunn, C. K.; Dunn, M. L.; Wang, T.; Jerry Qi, H. Recyclable 3D Printing of Vitrimer Epoxy. *Mater. Horiz.* **2017**, *4* (4), 598−607.

(13) Zhang, B.; Kowsari, K.; Serjouei, A.; Dunn, M. L.; Ge, Q. Reprocessable Thermosets for Sustainable Three-dimensional Printing. *Nat. Commun.* **2018**, *9* (1), 1831.

(14) He, H.; Lei, Z.; Zhang, W.; Yu, K. Recyclable 3D Printing of Polyimine-Based Covalent Adaptable Network Polymers. *3D Print. Addit. Manuf.* **2019**, *6* (1), 31−39.

(15) Yuan, T.; Zhang, L.; Li, T.; Tu, R.; Sodano, H. A. 3D Printing of a Self-healing, High Strength, and Reprocessable Thermoset. *Polym. Chem.* **2020**, *11*, 6441.

(16) Huang, L.; Jiang, R.; Wu, J.; Song, J.; Bai, H.; Li, B.; Zhao, Q.; Xie, T. Ultrafast Digital Printing toward 4D Shape Changing Materials. *Adv. Mater.* **2017**, *29* (7), 1605390.

(17) Heidarian, P.; Kouzani, A. Z.; Kaynak, A.; Paulino, M.; Nasri-Nasrabadi, B. Dynamic Hydrogels and Polymers as Inks for Three-Dimensional Printing. *ACS Biomater. Sci. Eng.* **2019**, *5* (6), 2688−2707.

(18) Wang, L. L.; Highley, C. B.; Yeh, Y.-C.; Galarraga, J. H.; Uman, S.; Burdick, J. A. Three-dimensional Extrusion Bioprinting of Single- and Double-network Hydrogels Containing Dynamic Covalent Crosslinks. *J. Biomed. Mater. Res., Part A* **2018**, *106* (4), 865−875.

(19) Kabb, C. P.; O'Bryan, C. S.; Deng, C. C.; Angelini, T. E.; Sumerlin, B. S. Photoreversible Covalent Hydrogels for Soft-Matter Additive Manufacturing. *ACS Appl. Mater. Interfaces* **2018**, *10* (19), 16793−16801.

(20) Miao, J.-T.; Ge, M.; Peng, S.; Zhong, J.; Li, Y.; Weng, Z.; Wu, L.; Zheng, L. Dynamic Imine Bond-Based Shape Memory Polymers with Permanent Shape Reconfigurability for 4D Printing. *ACS Appl. Mater. Interfaces* **2019**, *11* (43), 40642−40651.

(21) Fang, Z.; Song, H.; Zhang, Y.; Jin, B.; Wu, J.; Zhao, Q.; Xie, T. Modular 4D Printing via Interfacial Welding of Digital Light-Controllable Dynamic Covalent Polymer Networks. *Matter* **2020**, *2* (5), 1187−1197.

(22) Zhang, Z.; Corrigan, N.; Bagheri, A.; Jin, J.; Boyer, C. A Versatile 3D and 4D Printing System through Photocontrolled RAFT Polymerization. *Angew. Chem., Int. Ed.* **2019**, *58* (50), 17954−17963.

(23) Davidson, E. C.; Kotikian, A.; Li, S.; Aizenberg, J.; Lewis, J. A. 3D Printable and Reconfigurable Liquid Crystal Elastomers with Light-Induced Shape Memory via Dynamic Bond Exchange. *Adv. Mater.* **2020**, *32* (1), 1905682.

(24) Kelly, B. E.; Bhattacharya, I.; Heidari, H.; Shusteff, M.; Spadaccini, C. M.; Taylor, H. K. Volumetric Additive Manufacturing via Tomographic Reconstruction. *Science* **2019**, *363* (6431), 1075−1079.

(25) de Beer, M. P.; van der Laan, H. L.; Cole, M. A.; Whelan, R. J.; Burns, M. A.; Scott, T. F. Rapid, Continuous Additive Manufacturing by Volumetric Polymerization Inhibition Patterning. *Sci. Adv.* **2019**, *5* (1), eaau8723.

(26) Walker, D. A.; Hedrick, J. L.; Mirkin, C. A. Rapid, Large-volume, Thermally Controlled 3D Printing Using a Mobile Liquid Interface. *Science* **2019**, *366* (6463), 360−364.

(27) Bagheri, A.; Jin, J. Photopolymerization in 3D Printing. *ACS Appl. Polym. Mater.* **2019**, *1* (4), 593−611.

(28) Tumbleston, J. R.; Shirvanyants, D.; Ermoshkin, N.; Janusziewicz, R.; Johnson, A. R.; Kelly, D.; Chen, K.; Pinschmidt, R.; Rolland, J. P.; Ermoshkin, A.; Samulski, E. T.; DeSimone, J. M. Continuous Liquid Interface Production of 3D Objects. *Science* **2015**, *347* (6228), 1349−1352.

(29) Geng, Q.; Wang, D.; Chen, P.; Chen, S.-C. Ultrafast Multi-focus 3-D Nano-fabrication Based on Two-photon Polymerization. *Nat. Commun.* **2019**, *10* (1), 2179.

(30) Ding, R.; Du, Y.; Goncalves, R. B.; Francis, L. F.; Reineke, T. M. Sustainable Near UV-curable Acrylates Based on Natural Phenolics for Stereolithography 3D Printing. *Polym. Chem.* **2019**, *10* (9), 1067−1077.

(31) Medellin, A.; Du, W.; Miao, G.; Zou, J.; Pei, Z.; Ma, C. Vat Photopolymerization 3D Printing of Nanocomposites: A Literature Review. *J. Micro. Nanmanuf.* **2019**, *7* (3), 031006.

(32) Alifui-Segbaya, F.; Bowman, J.; White, A. R.; George, R.; Fidan, I.; Love, R. M. Chemical Characterization of Additively Manufactured Methacrylates for Dental Devices. *Addit. Manuf.* **2020**, *31*, 100944.

(33) Dall'Argine, C.; Hochwallner, A.; Klikovits, N.; Liska, R.; Stampf, J.; Sangermano, M. Hot-Lithography SLA-3D Printing of Epoxy Resin. *Macromol. Mater. Eng.* **2020**, *305* (10), 2000325.

(34) Deng, Y.; Li, J.; He, Z.; Hong, J.; Bao, J. Urethane Acrylate-based Photosensitive Resin for Three-dimensional Printing of Stereolithographic Elastomer. *J. Appl. Polym. Sci.* **2020**, *137* (42), 49294.

(35) Radchenko, A. V.; Duchet-Rumeau, J.; Gérard, J.-F.; Baudoux, J.; Livi, S. Cycloaliphatic Epoxidized Ionic Liquids as New Versatile Monomers for the Development of Shape Memory PIL Networks by 3D Printing. *Polym. Chem.* **2020**, *11* (34), 5475−5483.
(36) Lantean, S.; Roppolo, I.; Sangermano, M.; Pirri, C. F.; Chiappone, A. Development of New Hybrid Acrylic/Epoxy DLP-3D Printable Materials. *Inventions* **2018**, *3* (2), 29.
(37) Podgórski, M.; Mavila, S.; Huang, S.; Spurgin, N.; Sinha, J.; Bowman, C. N. Thiol−Anhydride Dynamic Reversible Networks. *Angew. Chem., Int. Ed.* **2020**, *59* (24), 9345−9349.
(38) Podgórski, M.; Spurgin, N.; Mavila, S.; Bowman, C. N. Mixed Mechanisms of Bond Exchange in Covalent Adaptable Networks: Monitoring the Contribution of Reversible Exchange and Reversible Addition in Thiol−Succinic Anhydride Dynamic Networks. *Polym. Chem.* **2020**, *11* (33), 5365−5376.
(39) Bartolo, P. J. *Stereolithography: Materials, Processes and Applications*; Springer Science & Business Media, 2011.
(40) Li, Z.; Wang, C.; Qiu, W.; Liu, R. Antimicrobial Thiol−ene−acrylate Photosensitive Resins for DLP 3D Printing. *Photochem. Photobiol.* **2019**, *95* (5), 1219−1229.
(41) Chen, L.; Wu, Q.; Wei, G.; Liu, R.; Li, Z. Highly Stable Thiol−ene Systems: From Their Structure−Property Relationship to DLP 3D Printing. *J. Mater. Chem. C* **2018**, *6* (43), 11561−11568.
(42) Oesterreicher, A.; Wiener, J.; Roth, M.; Moser, A.; Gmeiner, R.; Edler, M.; Pinter, G.; Griesser, T. Tough and Degradable Photopolymers Derived from Alkyne Monomers for 3D Printing of Biomedical Materials. *Polym. Chem.* **2016**, *7* (32), 5169−5180.
(43) Marx, P.; Romano, A.; Roppolo, I.; Chemelli, A.; Mühlbacher, I.; Kern, W.; Chaudhary, S.; Andritsch, T.; Sangermano, M.; Wiesbrock, F. 3D-Printing of High-κ Thiol-Ene Resins with Spiro-Orthoesters as Anti-shrinkage Additive. *Macromol. Mater. Eng.* **2019**, *304* (12), 1900515.
(44) Long, K. F.; Bongiardina, N. J.; Mayordomo, P.; Olin, M. J.; Ortega, A. D.; Bowman, C. N. Effects of 1°, 2°, and 3° Thiols on Thiol−Ene Reactions: Polymerization Kinetics and Mechanical Behavior. *Macromolecules* **2020**, *53* (14), 5805−5815.
(45) Hofstetter, C.; Orman, S.; Baudis, S.; Stampfl, J. Combining Cure Depth and Cure Degree: A New Way to Fully Characterize Novel Photopolymers. *Addit. Manuf.* **2018**, *24*, 166−172.
(46) Esfandiari, P.; Ligon, S. C.; Lagref, J. J.; Frantz, R.; Cherkaoui, Z.; Liska, R. Efficient Stabilization of Thiol-ene Formulations in Radical Photopolymerization. *J. Polym. Sci., Part A: Polym. Chem.* **2013**, *51* (20), 4261−4266.
(47) Podgórski, M.; Worrell, B. T.; Sinha, J.; McBride, M. K.; Bowman, C. N. Thermal Metamorphosis in (Meth)acrylate Photopolymers: Stress Relaxation, Reshaping, and Second-Stage Reaction. *Macromolecules* **2019**, *52* (21), 8114−8123.

https://dx.doi.org/10.1021/acsami.0c18979
ACS Appl. Mater. Interfaces 2021, 13, 12789−12796